ORIGINAL ARTICLE

American Journal of of Orthodontics and Dentofacial Orthopedics. 128(1): 16-26, 2005.

Assessment of mandibular growth and response to orthopedic treatment with 3-dimensional magnetic resonance images

Lucia H. S. Cevidanes,[a] Alexandre A. Franco,[b] Guido Gerig,[c] William R. Proffit,[d] Dennis E. Slice,[e] Donald H. Enlow,[f] Helio K. Yamashita,[g] Yong-Jik Kim,[h] Marco A. Scanavini[i], and Julio W. Vigorito[j]

Chapel Hill and Winston-Salem, NC, São Paulo, Brazil, and Cleveland, Ohio

Introduction: Three-dimensional (3D) craniofacial images are commonly used in clinical studies in orthodontics to study developmental and morphologic relationships. **Methods:** We used 3D magnetic resonance imaging to study relationships among craniofacial components during the pubertal growth spurt and in response to Fränkel appliance therapy. The sample for this prospective study was 156 high-resolution magnetic resonance images with 1 mm isotropic voxel resolution of 78 subjects taken initially (T1) and 18 $\pm$ 1 months (T2) after treatment or an observation period. The subjects were Brazilian children; 28 were treated and 25 were untreated for Class II malocclusion, and 25 were untreated with normal occlusions. A Procrustes geometric transformation of 3D skeletal landmarks was used to assess growth or treatment alterations from T1 to T2. The landmarks were located on the mandibular rami and the other craniofacial parts specifically related to the mandibular growth (the middle cranial fossae and the posterior part of the bilateral nasomaxilla). This allowed visualization of the entire volumetric dataset with an interactive 3D display. **Results:** Statistically significant differences were found in the relative 3D skeletal growth directions from T1 to T2 for treated vs untreated Class II children (Bonferroni-adjusted $P < .001$) and for treated Class II vs normal-occlusion subjects ($P < .001$). The major differences in the treated group were increased mandibular rami vertical dimensions and more forward rami relative to the posterior nasomaxilla and the middle cranial fossae. Principal component analysis made it possible to show individual variability and group differences in the principal dimensions of skeletal change. **Conclusions:** These methods are generalizable to other imaging techniques and 3D samples, and significantly enhance the potential of systematically controlled data collection and analysis of bony structures in 3 dimensions for quantitative assessment of patient parameters in craniofacial biology. (Am J Orthod Dentofacial Orthop 2005;128:16-26)

[a]Postdoctoral fellow, Department of Orthodontics, School of Dentistry, University of North Carolina, Chapel Hill.
[b]PhD program in Diagnostic Imaging, Paulista School of Medicine, UNIFESP, São Paulo, SP, Brazil.
[c]Taylor Grandy Professor of Computer Science and Psychiatry, University of North Carolina.
[d]Kenan Professor, Department of Orthodontics, University of North Carolina School of Dentistry.
[e]Assistant professor, Department of Biomedical Engineering, Wake Forest University School of Medicine, Winston-Salem, NC.
[f]Thomas Hill Emeritus Professor, Case Western Reserve University, Cleveland, Ohio.
[g]Professor, Department of Diagnostic Imaging Orthodontics, Paulista School of Medicine, UNIFESP, São Paulo, SP, Brazil.
[h]Research assistant, Department of Computer Science, University of North Carolina.
[i]Professor and chairman, Department of Orthodontics, Methodist University of São Paulo, São Bernardo, SP, Brazil.
[j]Professor and chairman, Department of Orthodontics, University of São Paulo, São Paulo, SP, Brazil.

CNPq, a Brazilian governmental agency for scientific and technological development, scholarship 20005-98/7, supported work by L.H.S.C. FAPESP-Brazil grant 97/01388-8 supported work by A.A.F., J.W.V., H.K.Y., and M.A.S. UNC Dental Research Center supported work by Y.K. and G.G. Work by D.E.S. was supported, in part, by the Austrian Ministry of Education, Science, and Culture, the Austrian Council for Science and Technology (grant AD 387/25-30 to Horst Seidler), Dr Edward G. Hill, and members of the Winston-Salem community.

Reprint requests to: Lucia H. S. Cevidanes, Department of Orthodontics, School of Dentistry, 201 Brauer Hall, University of North Carolina, CB#7450, Chapel Hill, NC 27599-7450; e-mail, cevidanl@dentistry.unc.edu

Submitted, September 2003; revised and accepted, March 2004.
0889-5406/$30.00

doi:10.1016/j.ajodo.2004.03.032

The application of 3-dimensional (3D) craniofacial imaging in carefully controlled prospective studies is a major advancement for new, meaningful diagnosis, developmental understanding, and treatment planning.[1-3] The ability to obtain accurate high-resolution volumetric datasets, a better understanding of the clinical value of 3D imaging, and easier-to-use workstations and software, and the need to integrate genetics and morphology have recently driven 3D techniques into the realm of commonly used and accepted clinical studies in orthodontics.[4,5]

Hans[6] described 3 areas of 3D imaging that are expected to have immediate impact in clinical practice: facial soft tissue surface mapping, digital models, and skeletal-structures assessment. Although new CT scanners rendering high-resolution images with low doses of radiation are the method of choice for evaluating skeletal structures,[7] recent work has been carried out to develop geometrically accurate magnetic resonance imaging (MRI) sequences that are suitable for the generation of 3D bone models.[8-10] This has been prompted by the move in medical imaging toward the use of MRI for controlled studies including untreated control and normal groups.[1] MRI is noninvasive, does not use ionizing radiation, has no known side effects, and provides multiplanar capabilities and excellent tissue contrast.[11]

Studies based on comparisons to population standard norms and 2-dimensional cephalometric representations of the 3D craniofacial structure cannot answer many questions regarding treatment response mechanisms and localization of enhanced growth of the mandible.[12-14] A challenge in using new "whole head" images is to capitalize on the understanding of the actual biology of growth. Three-dimensional measurements, landmark coordinates, curves, surface shape, or volume assessments might not show the morphogenesis of how the face actually grows if the analysis does not consider that mandibular response to orthopedic treatment occurs relative to other craniofacial structures,[15-18] and this is often not shown by changes in sample means.[19]

A workable interpretive system of the biology of craniofacial growth demands the assessment of the complex cause-and-effect interactions among bones growing simultaneously, but with differential timing.[13] Using a line such as sella-nasion to represent the cranial base completely misses the growth actions inferior to the middle cranial fossae. The midsagittal cranial base where basion, sella, or nasion are located is not developmentally related to mandibular growth. The bilateral maxillae articulate with the greater wings of the sphenoid in the middle cranial fossae.[20] Response to treatment and growth of the mandible occur relative to the middle cranial fossae and the posterior nasomaxilla, and the 3D craniofacial parts that articulate with the mandible and whose proportional growth keeps the facial pattern constant.

Locating 3D landmarks on complex curving structures is not a trivial problem.[21] As Bookstein[22] noted, there is a lack of literature about suitable operational definitions for the landmarks in the 3 planes of space (coronal, sagittal, and axial). The use of landmarks requires choices regarding the number, location, and definition of landmarks. Analyses of landmark data, in the study of growth changes and treatment effects, only describe landmark displacements relative to other landmarks.[22] Practical considerations of identification errors, coupled with an essential need for biological relevance and a balanced representation of counterpart components of the craniofacial form, limit the number and nature of landmarks available for analysis.[23]

The purpose of this study was to determine the actual 3D interrelationships among craniofacial bones at the beginning of the pubertal growth spurt and in response to Fränkel appliance therapy by using high-resolution MRI data. This prospective study evaluated whether 3D landmarks on the mandibular rami and its counterparts in the craniofacial structure recorded significant relative skeletal changes during the observation period when we compared the treated, untreated Class II, and normal-occlusion groups.

MATERIAL AND METHODS

Two of the authors (A.A.F. and L.H.S.C.) recruited the subjects and assessed them clinically at the Department of Orthodontics, Methodist University of São Paulo, Brazil. The screening involved clinical evaluation of children in neighborhood schools. The inclusion criteria specified white Brazilian children aged 9 to 12 years old, at the end of the mixed dentition, at the beginning of the pubertal growth spurt (in the ascendant part of the growth curve as evaluated by skeletal maturation in hand and wrist x-rays), with no early loss of deciduous teeth, and no absence of permanent teeth. Fifty-three subjects (28 boys, 25 girls) who met these criteria had clinical evaluations of Class II Division 1 malocclusions, with at least three-fourths cusp Class II molars and overjets between 4.5 and 10 mm; 25 subjects (9 boys, 13 girls) had normal occlusions, with molar relationships of Class I or edge-to-edge, canines in Class I, and overjets varying from 1 to 2.5 mm.

The Class II subjects were randomly allocated to 2 subgroups, treated and control, to avoid bias in the group comparison.[24] The treated group comprised 28 subjects treated with orthopedic appliancesfor mandibular advancement. The control group included 25 untreated subjects. The Class II controls received treatment after the 18-month observation period. The 25 normal-occlusion subjects served as a normal group for comparisons. At the start of the study, the mean ages were 10.3 $\pm$ 0.9 years for the treated group, 10.9 $\pm$ 0.7 years for the Class II control group, and 10.2 $\pm$ 0.8 years for the normal group.

The Fränkel Regulator II appliances were delivered within 15 days of the patients' initial records, and no other appliances were used during this phase. To

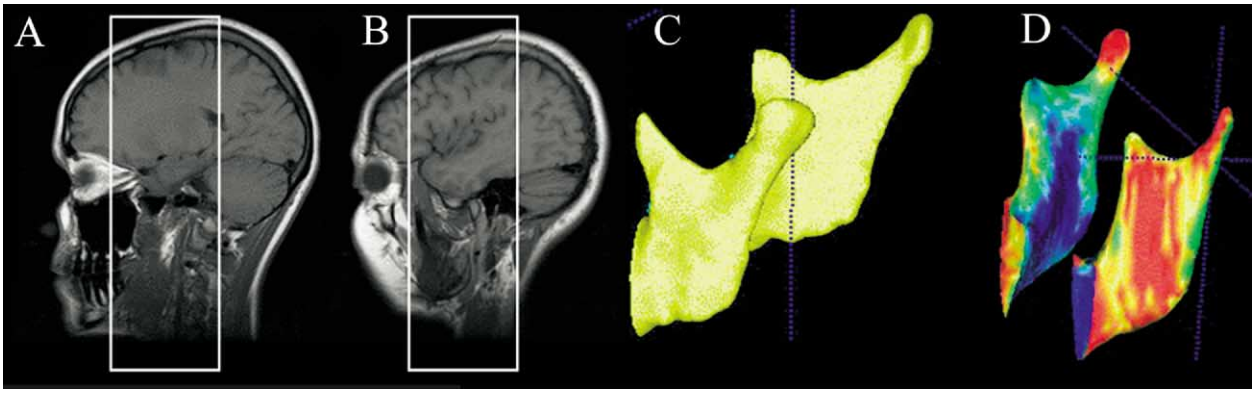

Fig 1. **A** and **B**, MRI sagittal localizer sections showing imaging area; **C**, mandibular rami 3D models with surface smoothing for visualization; **D**, visualization of relative superimposition of T1 and T2 structures in Valmet software[30] using spatial transformation based on 5 landmark pairs (Procrustes fit).

evaluate the stage of skeletal maturation of each hand-wrist radiograph according to the method described by Fishman,[25] we assessed the following selected ossification events: MP_3, the middle phalanx of the third finger, the epiphysis equals its diaphysis; and S stage, the first mineralization of the ulnar sesamoid bone.

The orthopedic treatment had an active period of 18 months to ensure an orthopedically stable occlusion with no shift from centric occlusion to maximum intercuspation. The clinical assessment was described by Cevidanes et al[26] previously.

One hundred fifty-six (2 x 78) MRI head scans from the 78 children (41 girls, 37 boys) were included in this study. The MRIs were taken at initial time periods (T1) and after 18 $\pm$ 1 months (T2). (From an initial sample of 90 children, 6 did not have the T2 scans, and the examination quality of another 6 subjects was compromised by anxiety.) The MRIs were acquired at the Department of Diagnostic Imaging, Paulista School of Medicine, Federal University of São Paulo, Brazil. A 0.5-tesla scanner (Signa, General Electric, Milwaukee, Wis) was used. The patients' teeth were in maximum intercuspation during the scan with a head coil. At T2, shifts from centric occlusion to maximum intercuspation were verified, and no subject had a shift. The MRI sequences for all 156 scans included a high-resolution 3D gradient echo acquisition with 1 mm isotropic voxel resolution, aiming for images with good geometric accuracy and clear tissue contrast between bone and surrounding soft tissues.[27,28] The imaging area comprised the middle cranial fossae, the posterior part of the nasomaxillary complex, and the mandibular rami (Fig 1).

All images were coded and their order permutated to keep the analyst blind to subject identification, group, and timing (T1 or T2). Visualization of sagittal, coronal, and axial cross-sections of the volumetric data set and a 3D graphical rendering of the volumetric mandibular rami was done with IRIS, an interactive image segmentation program[29,30] (Figs 1 and 2). IRIS allows tracking the (x, y) coordinate pair of an anatomical landmark selected in the z-plane window updating the x and y planes matching that coordinate (Fig 2).

Of the many regional craniofacial growth, remodeling, and displacement fields,[15-18,20] our analysis included identification and definition of 10 bilateral, 3D anatomic landmarks in the coronal, axial, and sagittal planes at the maxillary tuberosity, the mandibular condyle, the posterior and lower borders of the rami, and the greater wings of the sphenoid. The latter anatomically align with the nasomaxillary complex, marking the important anatomical and functional boundary between the nasomaxillary region and the common area comprising the pharynx, middle cranial floor, and rami[20] (Figs 3 and 4, Table I). The 3D coordinates of these landmarks were collected from the T1 and T2 scans of each subject. Many landmarks are what Bookstein[22] calls type III landmarks—points defined as "farthest" from other points—or, in this case, most superior, anterior, and so on with respect to anatomical axes. Most biologically useful information in such cases is confined to the direction in which the landmark definition is based. For this reason, each landmark was defined in each plane of space (Table I). Directions that were considered deficient are shown in Figure 3. Bookstein et al[31] provided an example of an analysis of 2-dimensional data taking such deficiency into account by letting landmarks "slide" along the

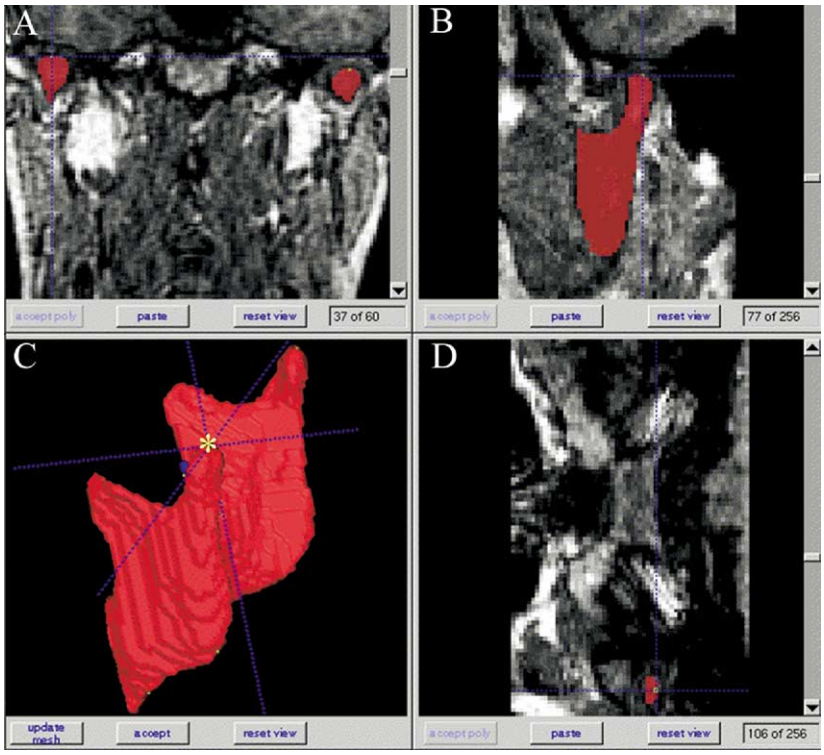

Fig 2. Visualization tool (IRIS 2000) used for location of ICo landmark as seen in **A**, coronal, **B**, sagittal, and **D**, axial cross-sections. **C**, 3D surface model of left and right mandibular rami displaying segmentation of 60 coronal slices 1 mm thick stacked together without smoothing.

appropriate directions before statistical comparison. In this study, we analyzed the landmarks as sets of fully 3D points.

Statistical analysis and error measurement

To assess measurement error and intraobserver variability, 10 landmarks were digitized from 4 MRIs (T1 and T2 for 2 subjects) on 5 separate occasions by each of 3 observers (graduate students) who were trained using images not included in the study as suggested by Ribeiro.[11] The 3D landmark coordinates for all data sets were superimposed by using generalized Procrustes analysis (GPA), and the total and within-image sums of squares were computed. The within-image sum of squares (0.009), including variation due to observer and within-observer measurement error, was about 17% of the total shape sum of squares (0.053), leaving 83% of total variation due to individual variability and the effect of time. These results show that the data used for this study were internally consistent and precise.

Multivariate analysis of the 3D landmark coordinates from 78 subjects at T1 and T2 was performed by standardized biometric approaches for sets of landmarks in 2 or 3 dimensions.[12,22,31,32] GPA was used to remove variability due to orientation, position, and size[32-34] among individual configurations of landmarks. To control the effect of position and size differences that could obscure variability in craniofacial form, each configuration of landmarks was first centered on the origin and scaled to unit centroid size (square root of the summed, squared coordinates after centering). Then, each configuration was rotated to align it with the sample mean configuration so that the sum of squared differences between corresponding landmark coordinates was minimal.[12,22,31,32] Because the sample mean is not estimable before GPA, 1 specimen was chosen as an initial estimate of the mean, all specimens fit to it, a new mean computed from the GPA data, and the process iterated until convergence.[35]

Permutation tests[12,31,32] were used to determine whether skeletal alterations with growth or response to treatment were differently distributed in the treated, untreated Class II, and normal-occlusion groups. The paired comparison design (the T1 and T2 scans formed a pair) was taken into account by using as data the differences in superimposed coordinates from T1 to T2 for each specimen. The rows of the design matrix were

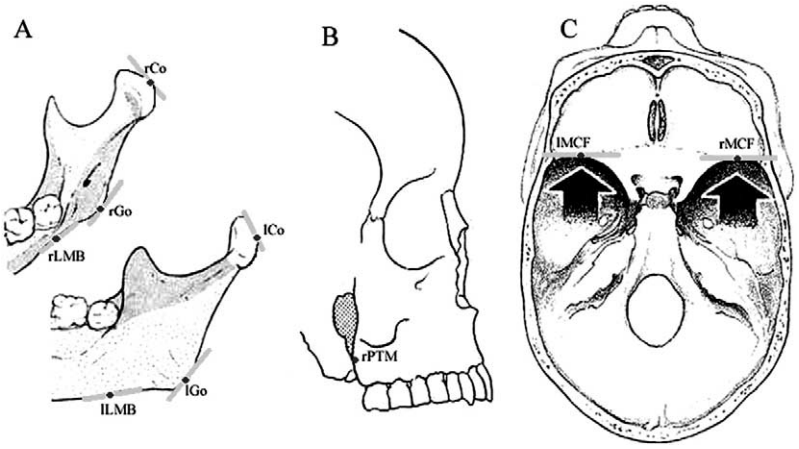

Fig 3. Landmark location. Landmarks indicated by points. Lines at some points indicate possible variation of landmark location. See Table I and text for details. **A**, rCo: right condylion; lCo: left condylion; rGo: right mandibular gonion; lGo: left mandibular gonion; rLMB: right lower border of mandibular corpus; lLMB: left lower border of mandibular corpus; **B**. PTM: pterygomaxillary (right PTM [rPTM] shown); and **C**, rMCF: right middle cranial fossa; lMCF: left middle cranial fossa.

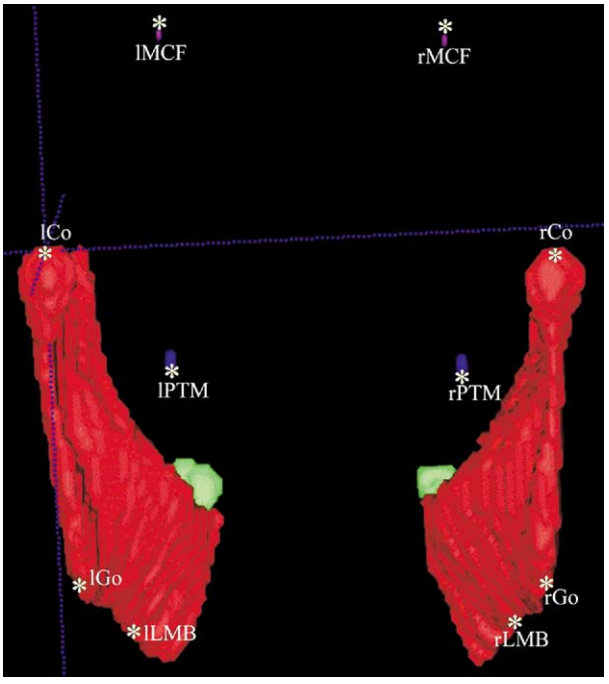

Fig 4. Landmark location on 3D models

permuted to create 999 pseudo-data sets in which group (treated vs untreated Class II vs normal occlusion) was randomly reassigned over the 78 subjects. The probability that a random permutation of this type results in a between-group sum of squares at least as great as the value actually observed is reported as the significance level (*P* value) of the association between the 3 groups and alterations between T1 and T2. The permutation tests were performed with the Morpheus et al morphometrics package.[36]

Deformation grids between T1 and T2 (Bookstein's thin-plate splines[12,21,22,31,32,37-40]) based on the configuration of 5 pairs of 3D landmarks were used for visualization of skeletal growth directions and mean group changes. The apparent displacement of landmarks and expansion or stretching (growth) and contraction (restriction or relative lesser amount of growth) areas as displayed with the deformation grids are all relative to the configuration of the landmarks used. The deformation grids show relative directions, not absolute size, of mandibular rami growth changes and response to treatment relative to the middle cranial fossae and posterior nasomaxilla landmarks.

Principal component analysis (PCA)[12,22,31,41,42] was carried out by using the covariance (not correlation) matrix of the coordinate differences used in the analysis. PCA is useful to provide maximally accurate, lower-dimensional representations of highly multivariate datasets. These principal components are the dimensions that best reproduce the distances between all data vectors by using linear combinations of the original coordinate differences. These components should not be thought of as factors causally responsible for the observed variation.

RESULTS

After we examined cross-sections of the volumetric data set and outlined the mandibular rami visible in these cross-sections, the segmented structures allowed

Table I. Landmark identification definitions: abbreviations and descriptions

		Landmark coordinates		
Landmark name	*Landmark abbreviation*	*X (left to right) sagittal view*	*Y (superior to inferior) axial view*	*Z (posterior to anterior) coronal view*
Right condylion	rCo	Middle point between posterior-superior -most and superior-posterior-most points of mandibular condyle, right side	Middle-posterior-most point of mandibular condyle, right side	Middle-superior-most point of mandibular condyle, right side
Left condylion	lCo	Middle point between posterosuperior-most and superoposterior-most points of mandibular condyle, left side	Middle-posterior-most point of mandibular condyle, left side	Middle-superior-most point of mandibular condyle, left side
Right mandibular gonion	rGo	Point at inferior border of mandibular angle at middistance between posterior-inferior-most point of ramus and inferior-posterior-most point of mandibular body, right side	Middle-posterior-most point of mandibular angle, right side	Middle-inferior-most point of mandibular angle, right side
Left mandibular gonion	lGo	Point at inferior border of mandibular angle at middistance between posterior-inferior-most point of ramus and posterior-inferior-most point of mandibular body, left side	Middle-posterior-most point of mandibular angle, left side	Middle-inferior-most point of mandibular angle, left side
Right lower mandibular border	rLMB	Point at inferior border of mandibular body below center of crown of second molar, right side	Middle-posterior-most point of mandibular body, right side	Middle-inferior-most point of mandibular body, right side
Left lower mandibular border	lLMB	Point at inferior border of mandibular body below center of crown of second molar, left side	Middle-posterior-most point of mandibular body, left side	Middle-inferior-most point of mandibular body, left side
Right middle cranial fossa	rMCF	Point in superior and endocranial surface where greater wing of sphenoid crosses anterior cranial floor at posterolateral bony wall of right orbit	Anterior-most point of middle cranial fossa (endocranial surface of greater wing of sphenoid), right side	Point in endocranial surface where greater wing of sphenoid crosses anterior cranial floor at lateral bony wall of right orbit
Left middle cranial fossa	lMCF	Point in superior and endocranial surface where greater wing of sphenoid crosses anterior cranial floor at posterolateral bony wall of left orbit	Anterior-most point of middle cranial fossa (endocranial surface of greater wing of sphenoid), left side	Point in endocranial surface where greater wing of sphenoid crosses anterior cranial floor at lateral bony wall of left orbit
Right pterygomaxillary	rPTM	Posterior limit of maxillary tuberosity at anterior-inferior-most point of pterygopalatine fissure (intersection of lateral pterygoid plate of sphenoid and pyramidal process of palatine bone), right side	Anterior-most point in vertex of V-shaped contour base of pterygopalatine fissure on axial view, right side	Medial-inferior-most point of pterygopalatine fissure, right side
Left pterygomaxillary	lPTM	Posterior limit of maxillary tuberosity at anterior-inferior-most point of pterygopalatine fissure (junction between lateral pterygoid plate of sphenoid and pyramidal process of palatine bone), left side	Anterior-most point in vertex of V-shaped contour of pterygopalatine fissure on axial view, left side	Medial-inferior-most point of pterygopalatine fissure, left side

visualization of the mandibular rami 3D models at T1 and T2 (Fig 5).

The color-coded deformation grids are graphic representations of truly 3D, relative (as determined by Procrustes fit) alterations from T1 to T2 in the craniofacial configuration of the structural counterparts where the 5 right and left landmark pairs are located (Fig 6).The plots show 2 dimensions, and the colors show the third dimension.

A sagittal view of the 3D deformation grids shows the changes in mean landmark configuration from T1 to T2 without magnification for the untreated Class II control (Fig 7, *A*), treated (Fig 7, *B*), and normal-occlusion groups (Fig 7, *C*). The alterations in the untreated Class II control and normal-occlusion group means show little deformation and indicate the maintenance of the location of craniofacial landmarks relative to each other with growth. For the treated group

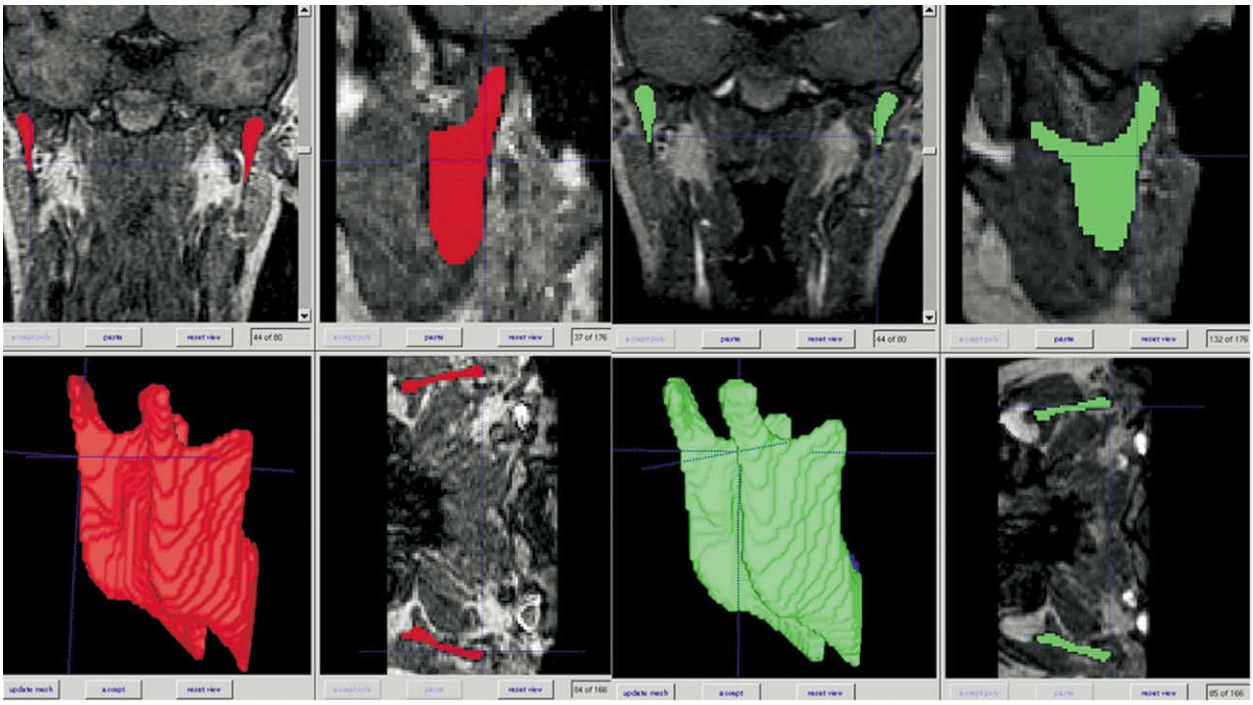

Fig 5. Mandibular rami segmented at T1 (*red*) and T2 (*green*).

(Fig 7, *B*), the coronal and axial gridlines show the more forward (anterior) alignment and increased vertical dimension of the mandibular rami relative to their counterparts: the posterior nasomaxilla and the middle cranial fossae. The more anterior rami alignment is shown by a relatively more anterior bending of the coronal gridlines, while the axial gridlines shift anteriorly, at the gonion landmarks, compared with a relative posterior bending of the coronal gridlines, while the axial gridlines shift anteriorly, at the condylion landmarks. Increased rami vertical dimension is shown by a relatively more inferior bending of the axial gridlines, while the coronal gridlines shift inferiorly at the gonion landmarks, compared with a relatively superior bending, and the axial gridlines shift anteriorly at the condylion landmarks.

The significance of the skeletal alterations visualized in the deformation grids was determined by permutation tests (Table II). As the lower mandibular border landmarks were defined relative to the root of the second molars, tooth movement affected their displacement with growth and treatment. To assess purely skeletal alteration, we refitted and tested the data, excluding the lower mandibular border landmarks. Changes in the configuration of the mandibular rami relative to the middle cranial fossae and pterygomaxillary landmarks showed highly significant differences between the treated and untreated Class II controls ($P < .001$), and the treated and normal-occlusion groups ($< .001$). The growth changes in the untreated Class II controls were comparable with those in the normal-occlusion group (nonsignificant difference, $P < .2$).

PCA applied to landmark-coordinate differences (excluding lower mandibular border) assessed the principal dimensions and individual variability in skeletal alterations from T1 to T2. Figure 8 shows the scattergrams of the first 2 principal components for the full 78-subject data set. These principal components represent 28% and 15% of total sample variability, respectively. These scattergrams refer to the pattern of relatively greatest variability in skeletal alterations; each stands for a set of correlated shifts of all landmarks jointly in each subject. The patterns of skeletal alterations for the treated subjects clearly differ from those of the untreated Class II and the normal-occlusion subjects.

DISCUSSION

This study was the first to apply high-resolution 3D MRI data for a clinically relevant diagnostic interpretation of orthopedic treatment and skeletal growth changes in a prospective and systematically controlled investigation. We applied generalizable methods for 3D

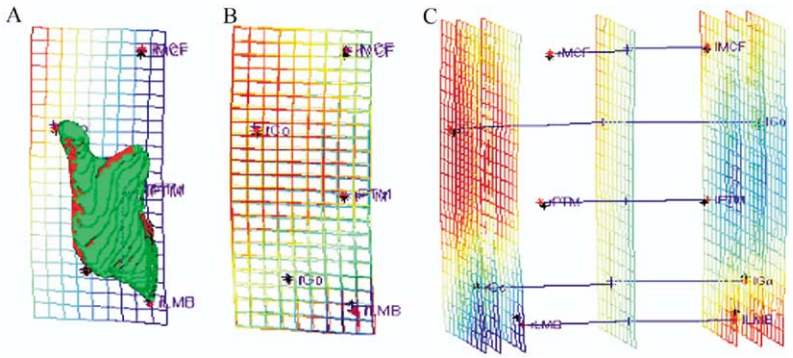

Fig 6. Visualization of relative 3D skeletal growth directions between T1 and T2 for patient in treated group using color-coded 3D deformation gridlines. **A**, Display of 1 of 256 sagittal planes, with axial (inferosuperior) and coronal (anteroposterior) deformation gridlines. Right (*r*) and left (*l*) landmarks appear superimposed because this patient did not have asymmetry. Color-coding red to blue indicates, respectively, left to right sagittal location of each landmark relative to plane chosen for visualization. T1 and T2 bilateral landmarks are shown as black and red asterisks, respectively. **B**, Multiple coronal/axial grids as seen from sagittal perspective. **C**, Rotated frontal view of 7 different sagittal planes.

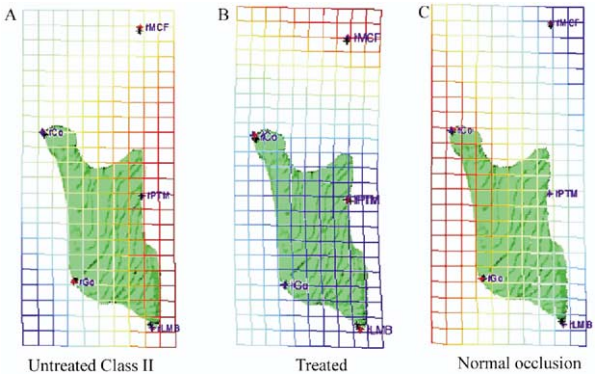

Fig 7. Deformation grids of mean alterations in relative 3D skeletal growth directions between T1 and T2 for untreated Class II control, treated Class II, and normal occlusion groups, without magnification. For visualization purposes, only 1 sagittal plane is displayed with axial (inferosuperior) and coronal (anteroposterior) deformation gridlines; color code red-blue indicate sagittal (medial- lateral) landmark displacement. Note greater deformation of mean grid for treated group (B).

Table II. *P* values from Bonferroni-adjusted, pairwise permutation tests of 3D skeletal landmark displacements between T1 and T2

Group	*Treated*	*Untreated Class II controls*	*Normal occlusion*
Treated	—		
Untreated Class II controls	0.001*	—	
Normal occlusion	0.001*	0.200	—

landmark data, focusing on the morphogenic basis of Class II malocclusion. For functional and anatomic balance in the correction of the maxillary/mandibular discrepancy of patients in whom the mandible is retrognathic, alteration of the growth of the mandibular rami, relative to its equivalents in the upper face structure, is the biologic target.[15,17,26] The biologic question of whether mandibular rami growth is altered relative to its equivalents was addressed by 3D landmarks at skeletal counterparts that articulate with each other during growth. Specifically, we assessed how the mandibular rami can be altered relative to how far anteriorly the middle cranial fossae place the nasomaxillary complex and also how widely it places the 2 condyles bilaterally.

The standard biometric approach of Procrustes fit applied in this study for T1 to T2 comparisons was not aimed at an exact modeling of craniofacial growth, for which the only valid method would be the use of intraosseous implants.[17,43] More than a description relative to stable intraosseous reference points like implants, the purpose of this study was to analyze the relative displacement of key counterpart components during growth and response to treatment. Therefore, the Procrustes fit of each subjects' landmark coordinates showed the displacement of landmarks relative to all landmarks included in the 3D models, controlling for the variations in rotation, translation, and scale.[44]

Not only were the principal dimensions of skeletal

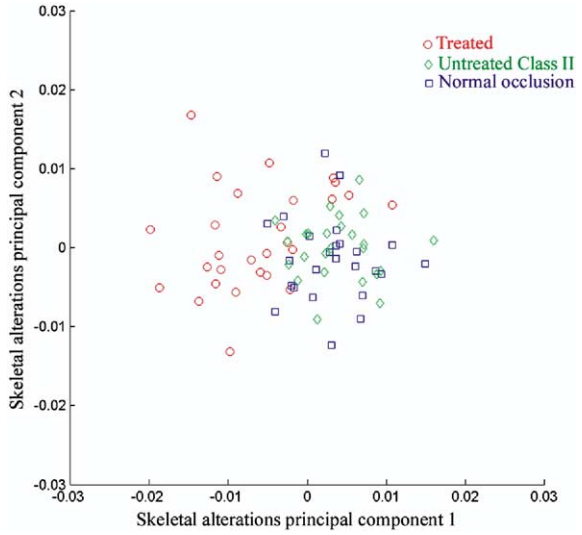

Fig 8. Scattergrams of first 2 skeletal alterations (T2-T1) principal components for landmark data set.

alterations different for treated and untreated Class II and normal-occlusion subjects, but also the PCA scattergrams showed considerable individual variability in growth and response to treatment alterations. Clinical decisions such as the optimal time to start treatment are inevitably difficult because of the variability between patients and the uncertainty about growth and treatment response.[45]

A remarkable product of this study was the visualization of the underlying 3D patterns of relative skeletal alterations of the mandibular rami by using deformation grids. The nonsignificant configuration changes from T1 to T2 in both the untreated Class II control and the normal-occlusion deformation grids showed maintenance of the landmark configuration with growth, with slight relative mandibular advancement, characteristic of the differential maxillary/mandibular growth at the beginning of the pubertal growth spurt. For the treated group, the skeletal alterations visualized in the T1-T2 deformation grids were highly significantly different (treated vs untreated Class II controls $P < .001$, and treated vs normal occlusion $P < .001$). The differential anteroposterior location of 3D landmarks observed in the deformation of coronal/axial gridlines showed more forward (anterior) rami alignment relative to their counterparts in the posterior nasomaxilla and the middle cranial fossae. The deformation grids also showed differential vertical location of landmarks with increased relative mandibular rami vertical dimension.

The striking statistically significant 3D skeletal alterations shown graphically by the deformation grids are considered a favorable skeletal response to treatment with the Fränkel Regulator II, aimed at increased relative mandibular growth. The results of this study corroborate our findings by using Enlow's counterpart analysis in 2-dimensional cephalograms, although those cannot address whether early treatment provides enough additional benefit to justify the almost inevitable greater burden of a 2-phase treatment.[46]

For 2 decades, Baumrind[2] and Baumrind et al[47] have discussed the need for 3D morphometric methods to analyze the configuration of craniofacial morphology, but 3D comparative studies based on statistical standard values or shape alterations can also be subject to errors and misinterpretations of the biology of growth. A dangerous situation in our science is created by the availability of powerful computers and software packages that can be used with little comprehension of the biology of craniofacial morphogenesis and the mathematical basis of the approaches. Franchi et al[39] described improved methods for assessing craniofacial morphology changes such as finite element methods,[43,48] Euclidean distance matrix analysis,[23,38] elliptical Fourier functions,[49] and Bookstein's innovations (tensor analysis,[50] shape coordinates,[51] and thin-plate splines[37-40]), but these methods have not yet been applied to evaluate the actual anatomical interactions between the different craniofacial structures during growth.

In our study, we applied higher-power statistical methods for 3D landmark coordinates,[34] in contrast to the traditional multivariate analysis of selected distance measurements, angles, and ratios based on landmarks. The pioneering studies of Bookstein[12,22] and Bookstein et al[31] described landmark locations as image features but emphasized that, as a set, they constitute a stringent abstraction from medical images. Because landmarks do not contain information on the spaces, curves, or surfaces between them, landmark displacement can only be described relative to the other landmarks, ie, outcome measurements in any method only describe relative displacement.[23]

The outstanding studies of Subsol et al[10] and Andresen et al[41] provide clear advances toward studies of curves or surfaces in 3D, referring to tens of thousands of 3D points to define geometry. Andresen et al[41] and Mitteroecker et al[52] provide glimpses of how future studies with semi-landmarks on the surface might incorporate information about deficient direction in landmark definition into the analysis of 3D data such as those considered here. However, the information from curves and surfaces must also be guided by the manner of assembly of craniofacial complex components during growth. Subsol et al[10] described the need to compute a condensed set of about 20 to 30 mean-

ingful shape parameters to obtain a more compact and easy way to understand the representation. Nevertheless, the biologic problem is that shapes of bones are not the primary causes of skeletal discrepancies. It is what causes the fitting or nonfitting, and the retrusions or protrusions, that matters for understanding the actual, direct reasons for individual facial form, growth, and response to treatment.[20] When the landmarks chosen for an analysis span many skeletal components that articulate, variation describing the position of landmarks on 1 structure relative to another is also present in the data.[23] The entire bony rami and their adaptable condyles provide the fitting of the mandible to the nasomaxilla and the basicranium.[15,20] They can receive developmental signals from masticatory muscles, pharyngeal muscles, genial muscles, tongue, facial musculature, integument, mucosa, dentition, and all components of the servosystem.[18] These signaling processes activate the osteogenic and chondrogenic tissues to regionally develop the growing shape and size throughout the rami and mandible as a whole. According to the counterpart concept, the posterior breadth of the rami adapt to the posteroanterior size of its counterpart, which is the pharyngeal space determined by the size of the temporal lobes and the middle cranial fossae. The vertical rami similarly adapt to the vertically growing nasomaxillary complex and the vertical length of the middle cranial fossae.[20] If head-form or breathing and swallowing variations are regionally imbalanced, the rami compensatory function can come into play and provide offsetting developmental responses, reducing the severity of a malocclusion.[15] The counterpart concept applied in this 3D study pinpoints the particular combination of anatomic and developmental factors underlying malocclusions and other anomalies.

CONCLUSIONS

This article describes a methodology for the assessment of growth and treatment changes in the morphology and morphogenic assembly of the 3D craniofacial structure. These methods analyze the relationship of meaningful biological landmarks and morphologic events during a person's growth, without comparisons to population standard norms. The 3D deformation grids of thin-plate splines from T1 to T2 allowed visualization of highly significant skeletal alterations of the mandibular rami relative to the middle cranial fossae and posterior maxillary landmarks in the treated group, with a more forward alignment and increased vertical rami dimension.

This methodology is generalizable and can be applied to other imaging modalities, such as computerized tomography scans. We can now evaluate the 3D craniofacial assembly with a truly biologic means of identifying the underlying factors that determine a patient's craniofacial anatomy and development.

We thank Dr Fred L. Bookstein for his invaluable assistance in the multivariate aspects of this work and Dr Kurt Faltin, Jr, for his contribution and discussions in the clinical assessment of the Fränkel appliance.

REFERENCES

1. Arens R, McDonough JM, Corbin AM, Rubin NK, Carroll ME, Pack AI, et al. Upper airway size analysis by magnetic resonance imaging of children with obstructive sleep apnea syndrome. Am J Respir Crit Care Med 2003;167:65-70.
2. Baumrind S. Commentary. Am J Orthod Dentofacial Orthop 2002;121:29-30.
3. Kusnoto B, Evans CA. Reliability of a 3D surface laser scanner for orthodontic applications. Am J Orthod Dentofacial Orthop 2002;122:342-8.
4. Roush W. A womb with a view. Science 1997;278:1397-9.
5. Trelease RB. Anatomical informatics: millennial perspectives on a newer frontier. Anat Rec 2002;269:224-35.
6. Hans M. Ask us. Am J Orthod Dentofacial Orthop 2002;122(4): 14A.
7. Mozzo P, Procacci C, Tacconi A, Martini PT, Andreis IA. A new volumetric CT machine for dental imaging based on the cone-beam technique: preliminary results. Eur Radiol 1998;8:1558-64.
8. Sgouros S, Natarajan K, Hockley AD, Goldin JH, Wake M. Skull base growth in childhood. Pediatr Neurosurg 1999;31:259-68.
9. Stindel E, Udupa JK, Hirsch BE, Odhner D, Couture C. 3D MR image analysis of the morphology of the rear foot: application to classification of bones. Comput Med Imaging Graph 1999;23: 75-83.
10. Subsol G, Thirion JP, Ayache N. A scheme for automatically building three-dimensional morphometric anatomic atlases: application to a skull atlas. Med Image Anal 1998;2:37-60.
11. Ribeiro RF. Avaliação estrutural da ATM em crianças e adultos jovens assintomáticos a través de imagens por ressonância magnética [tese]. Bauru, Brazil: University of São Paulo; 1996.
12. Bookstein FL. Shape and the information in medical images: a decade of the morphometric synthesis. Comput Vis Image Understanding 1997;66:97-118.
13. Enlow D. Discussion. Am J Orthod Dentofacial Orthop 2000; 117:147.
14. Harrell WE Jr, Hatcher DC, Bolt RL. In search of anatomic truth: 3-dimensional digital modeling and the future of orthodontics. Am J Orthod Dentofacial Orthop 2002;122:325-30.
15. Bhat M, Enlow DH. Facial variations related to headform type. Angle Orthod 1985;55:269-80.
16. Björk A, Skieller V. Contrasting mandibular growth and facial development in long face syndrome, juvenile rheumatoid polyarthritis, and mandibulofacial dysostosis. J Craniofac Genet Dev Biol (Suppl) 1985;1:127-38.
17. Björk A, Skieller V. Normal and abnormal growth of the mandible. A synthesis of longitudinal cephalometric implant studies over a period of 25 years. Eur J Orthod 1983;5:1-46.
18. Petrovic A, Stutzmann J, Lavergne J. Mechanism of craniofacial growth and modus operandi of functional appliances: a cell-level and cybernetic approach to orthodontic decision making. In: Carlson DS, editor. Craniofacial growth theory and orthodontic

treatment. Monograph 23. Craniofacial Growth Series. Ann Arbor: Center for Human Growth and Development; University of Michigan; 1990. p. 13-74.
19. Ghafari J, Baumrind S, Efstratiadis SS. Misinterpreting growth and treatment outcome from serial cephalographs. Clin Orthod Res 1998;1:102-6.
20. Enlow DH, Kuroda T, Lewis AB. The morphologic and morphogenetic basis for craniofacial form and pattern. Angle Orthod 1971;41:161-88.
21. Dean D, Hans MG, Bookstein FL, Subramanyan K. Three-dimensional Bolton-Brush Growth Study landmark data: ontogeny and sexual dimorphism of the Bolton Standards cohort. Cleft Palate Craniofac J 2000;37:145-55.
22. Bookstein FL. Morphometric tools for landmark data. 1st ed. Cambridge: Cambridge University Press; 1991. p. 435.
23. Richtsmeier JT, Deleon VB, Lele SR. The promise of geometric morphometrics. Yearbook Phys Anthropol 2002;45:63-91.
24. Phillips C, Tulloch C. The randomized clinical trial as a powerful means for understanding treatment efficacy. Sem Orthod 1995; 1:128-38.
25. Fishman LS. Radiographic evaluation of skeletal maturation. Angle Orthod 1982;52:88-112.
26. Cevidanes LHS, Franco AA, Scanavini MA, Enlow DH, Vigorito JW, Proffit WR. Clinical outcomes of Fränkel appliance therapy assessed with counterpart analysis. Am J Orthod Dentofacial Orthop 2003;123:379-87.
27. Disler DG, Marr DS, Rosenthal DI. Accuracy of volume measurements of computer tomography and magnetic resonance imaging phantoms by three-dimensional reconstruction and preliminary clinical application. Invest Radiol 1994;29:739-45.
28. Sumanaweera TS, Glover GH, Binford TO, Adler MR Jr. Susceptibility misregistration correction. IEEE Trans Med Imaging 1993;12:251-9.
29. Gilmore JH, Gerig G, Specter B, Charles C, Wilber J, Herzberg B, et al. Neonatal cerebral ventricle volume: a comparison of 3D ultrasound and magnetic resonance imaging, Ultrasound Med Biol 2001;27:1143-6.
30. Gerig G, Jomier M, Chakos M. Valmet: a new validation tool for assessing and improving 3D object segmentation. In: Niessen W, Viergever M, editors. MICCAI 2001: Proceedings of the International Society and Conference on Medical Image Computing and Computer-Assisted Intervention; 2001 Oct 14-17; Utrecht, Netherlands. Berlin: Springer; 2001. p. 516-28.
31. Bookstein FL, Schafer K, Prossinger H, Seidler H, Fieder M, Stringer C, et al. Comparing frontal cranial profiles in archaic and modern homo by morphometric analysis. Anat Rec 1999; 257:217-24.
32. Gharaibeh WS, Rohlf FJ, Slice DE, DeLisi LE. A geometric morphometric assessment of change in midline brain structural shape following a first episode of schizophrenia. Biol Psychiatry 2000;48:398-405.
33. Dryden IL, Mardia KV. Statistical shape analysis. John Wiley & Son; New York: 1998.
34. Rohlf FJ. Statistical power comparisons among alternative morphometric methods. Am J Phys Anthropol 2000;111:463-78.
35. Gower JC. Generalized Procrustes analysis. Psychometrika 1975;40:33-51.
36. Slice DE. Morpheus et al: software for morphometric research. Revision 1-30-98. Stony Brook (NY): State University of New York, Department of Ecology and Evolution; 1998. (Recent beta).
37. Baccetti T, Franchi L, McNamara JA Jr, Thin-plate spline analysis of treatment effects of rapid maxillary expansion and face mask therapy in early Class III malocclusions. Eur J Orthod 1999;21:275-81.
38. Cerajewska TL, Sing GD. Morphometric analysis of the mandible in prepubertal craniofacial microsomia patients treated with an inverted-L osteotomy. Clin Anat 2002;15:100-17.
39. Franchi L, Baccetti T, McNamara JA Jr. Thin-plate spline analysis of mandibular growth. Angle Orthod 2000;71:83-9.
40. Lux CJ, Rubel J, Starke J, Conradt C, Stellzig A, Komposch G. Effects of early activator treatment in patients with Class II malocclusion evaluated by thin-plate spline analysis. Angle Orthod 2000:71:120-6.
41. Andresen R, Bookstein FL, Conradsen K, Ersboll BK, Marsh JL, Kreiborg S. Surface-bounded growth modeling applied to human mandibles. IEEE Trans Med Imaging 2000;19:1053-63.
42. Shenton ME, Gerig G, McCarley RW, Szekely G, Kikinis R. Amygdala-hippocampal shape differences in schizophrenia: the application of 3D shape models to volumetric MR data. Psychiatry Res 2002;115:15-35.
43. Melsen B, Dalstra M. Distal molar movement with Kloehn headgear: is it stable? Am J Orthod Dentofacial Orthop 2003; 123:374-8.
44. Slice DE. Landmark coordinates aligned by Procrustes analysis do not lie in Kendall's shape space. Syst Biol 2001;50:141-9.
45. Chen JY, Will LA, Niederman R. Analysis of efficacy of functional appliances on mandibular growth. Am J Orthod Dentofacial Orthop 2002;122:470-6.
46. Proffitt WR, Tulloch JFC. Preadolescent Class II problems: treat now or wait? Am J Orthod Dentofacial Orthop 2002;121:560-2.
47. Baumrind S, Moffitt FH, Curry S. The geometry of three-dimensional measurement from paired coplanar x-ray images. Am J Orthod 1983;84:313-22.
48. Singh GD, Clark WJ. Localization of mandibular changes in patients with Class II Division 1 malocclusions treated with Twin-block appliances: finite element scaling analysis. Am J Orthod Dentofacial Orthop 2001;119:419-25.
49. Ferrario VF, Sforza C, Guazzi M, Serrao G. Elliptic Fourier analysis of mandibular shape. J Craniofac Genet Dev Biol 1996;16:208-17.
50. McNamara JA, Bookstein FL, Shaughnessy TG. Skeletal and dental changes following function regulator therapy in Class II patients. Am J Orthod 1985;88:91-110.
51. Franchi L, Baccetti T, McNamara JA. Shape-coordinate analysis of skeletal changes induced by rapid maxillary expansion and facial mask therapy. Am J Orthod Dentofacial Orthop 1998;114: 418-26.
52. Mitteroecker P, Gunz P, Bookstein FL. Semilandmarks in three dimensions. In: Slice DL, editor. Modern morphometrics in physical anthropology. New York: Kluwer Academic Publishers: 2004.